The Astrophysical Journal, 644:464–474, 2006 June 10

THE REMARKABLE FAR-ULTRAVIOLET SPECTRUM OF FK COMAE BERENICES: KING OF SPIN

Thomas R. Ayres, Graham M. Harper, and Alexander Brown
Center for Astrophysics and Space Astronomy, University of Colorado, 389 UCB, Boulder, CO 80309-0389;
ayres@casa.colorado.edu, gmh@casa.colorado.edu, ab@casa.colorado.edu

Heidi Korhonen and Ilya V. Ilyin
Astrophysikalisches Institut Potsdam, An der Sternwarte 16, 14482 Potsdam, Germany;
hkorhonen@aip.de, ilyin@aip.de

Seth Redfield[1]
McDonald Observatory, University of Texas, 1 University Station,
Austin, TX 78712-0259; sredfield@astro.as.utexas.edu

and

Brian E. Wood
JILA, University of Colorado and NIST, 440 UCB, Boulder, CO 80309-0440; woodb@origins.colorado.edu
Received 2005 December 1; accepted 2006 February 7

ABSTRACT

A *Far Ultraviolet Spectroscopic Explorer* (*FUSE*) pointing on the ultrafast rotating yellow giant FK Comae Berenices (HD 117555; $v \sin i \sim 163$ km s^{-1}) recorded emission profiles of C III λ977 ($T \sim 8 \times 10^4$ K) and O VI λ1031 ($T \sim 3 \times 10^5$ K) that are exceptionally broad and asymmetric, but nearly identical in shape, aside from a blueward absorption component in the latter (identified as interstellar O I, rather than, say, a C III outflow feature). The FWHMs exceed 500 km s^{-1}, *twice* the broadest far-UV line shape of any normal late-type star observed to date, but similar to the Hα profiles of FK Com, and following the trend of other fast spinning early G giants that often display "superrotational" broadening of their UV "hot" lines. Although the red-asymmetric O VI λ1031 profile is suggestive of an outflow at $\sim 3 \times 10^5$ K, the weaker member of the doublet, λ1037, does not display the differential absorption pattern expected from a warm wind. Furthermore, at times the chromospheric Mg II λ2796 + λ2803 composite profile, from a collection of *International Ultraviolet Explorer* (*IUE*) echellegrams obtained two decades earlier, is nearly identical in shape to red-asymmetric O VI λ1031. A contemporaneous optical Doppler map places the photospheric dark spots mainly in the polar regions of the approaching hemisphere. The dominantly redward biased profiles of C III and O VI could be explained if the associated emission zones were *leading* the starspots in phase and partially rooted in lower latitudes.

Subject headings: stars: coronae — stars: individual (HD 117555, HD 111812, HD 113001B, vZ 1128) — ultraviolet: stars

Online material: color figures

1. INTRODUCTION

FK Comae Berenices (HD 117555) is a rapidly rotating yellow giant, in an eponymous class, whose members display spectacular emission activity from X-rays to radio (Bopp & Stencel 1981). Merrill (1948) originally called attention to the remarkably wide Hα emission of FK Com ($\sim$1000 km s^{-1} at the base), conspicuous even in the discovery objective prism photographs. He attributed the anomalous broadening to "prominence-like motion" in an equatorial ring of gas, flung away from the star by its fast rotation. By its color and luminosity, FK Com is one of the relatively rare objects that fall in the Hertzsprung gap, sporadically populated by moderate-mass stars during the brief "first crossing" phase of their initial post–main-sequence evolution. While FK Com shares some similarities with normal Hertzsprung gap giants, including ultrafast rotation, a depressed X-ray/C IV index, and unevolved N/C abundance ratio (Ayres et al. 1998 and references therein, hereafter A98), it is rotating close to breakup (with $v \sin i = 163 \pm 4$ km s^{-1}; see Huenemoerder et al. 1993, hereafter H93), nearly twice as fast as the upper end of the normal yellow giant spin distribution. In fact, the present angular momentum is thought to exceed that possible for a $\sim 2\ M_\odot$ main-sequence progenitor (appropriate to the current luminosity of FK Com; see H93), while its space motion and moving group membership are old disk, contrary to normal moderate-mass stars that ordinarily would belong to a young disk population (Guinan & Robinson 1986). The popular model to explain these discrepancies, anticipated by Webbink (1976), suggested for the particular case of FK Com by Bopp & Rucinski (1981), and later embellished by Ramsey et al. (1981), H93, and others, is that FK Com is a recent merger of two old solar-mass dwarfs, previously a W Ursae Majoris contact binary.

While its origin is strikingly different from normal denizens of the Hertzsprung gap, FK Com potentially can serve as a surrogate for the events that take place when these fast rotating giants begin to develop deep convection zones and associated strong magnetic activity through a solar-like "dynamo" (Parker 1970). (However, one must be wary if the merger was very recent because an "excretion" disk remnant of the disrupted secondary might still persist, as speculated by Webbink 1976.)

As for the normal moderate-mass giants, they begin to display symptoms of strong solar-like magnetic activity, i.e., prominent

[1] Hubble Fellow.

TABLE 1
STELLAR PROPERTIES

Name	Spectral Type	(l, b) (deg)	d (pc)	V (mag)	$B-V$ (mag)	v_r (km s^{-1})	$v \sin i$ (km s^{-1})	References
FK Com (HD 117555)	$\gtrsim$G2 III	(17.0, +80.7)	230 ± 60	+8.2	+0.9	−24 ± 3	163 ± 4	1
31 Com (HD 111812)	G0 III	(115.0, +89.6)	94 ± 8	+4.9	+0.6	−1 ± 3	60 ± 3	2, 3
HD 113001B	sdO	(111.0, +81.2)	220 ± 90	+10.7	−0.5	−9	<20	4, 5
vZ 1128	O8p	(42.5, +78.7)	10^4	+14.9	−0.3	−151 ± 8	<25	6

NOTES.—From SIMBAD, as supplemented by references listed in the last column. The $v \sin i$ limits for the two sdO stars were based on the appearance of their narrow absorption features in the *FUSE* spectra.

REFERENCES.—(1) H93; (2) de Medeiros & Mayor 1995; (3) Strassmeier et al. 1990; (4) Fabricius & Makarov 2000; (5) Makarov & Fabricius 1999; (6) Howk et al. 2003.

far-ultraviolet (FUV) C IV λ1550 emission ($T \sim 10^5$ K) and kilovolt soft X-rays ($T \sim 10^6$–10^7 K), when they first become convective, upon crossing rapidly through the F spectral types. However, these Hertzsprung gap stars exhibit a puzzling "X-ray deficiency" (X-ray/C IV flux ratios as little as 10% those of cooler giants; Simon & Drake 1989) and "superrotational broadening" of their hot UV features (like C IV), with line widths up to *twice* those expected from the photospheric $v \sin i$ (A98).

Toward the red side of the gap, in the mid-G spectral types, the rotation rates of giants suddenly plummet (Gray 1981), in a narrow region called the rapid braking zone (RBZ). Ironically, the precipitous spin-down likely comes about by the *strengthening* of dynamo action as the evolving convection zone deepens. Although the corona intensifies temporarily, magnetic wind braking, particularly if accompanied by frequent flare-associated mass ejections, can be highly effective in giant stars (e.g., Ayres et al. 1999), and very soon the stellar spin, the dynamo, and its attendant activity would fade. The transition between the X-ray–deficient gap giants and their slightly further advanced counterparts in the intense and short-lived RBZ phase would seem to be an important place to seek answers concerning the evolution of coronal activity in giants and the operation of the dynamo mechanism under extreme conditions. Unfortunately, stars in this crucial evolutionary stage are rare. Thus, a proxy like FK Com is especially valuable.

Here we describe the 920–1180 Å spectrum of FK Com, as captured by the *Far Ultraviolet Spectroscopic Explorer* (*FUSE*), and speculate on possible causes of the remarkable emission-line shapes of multiply ionized carbon and oxygen that were recorded.

2. OBSERVATIONS

Table 1 lists basic properties of FK Com. Also included is a comparison Hertzsprung gap giant 31 Comae (HD 111812; G0 III) and two O-type subdwarfs, HD 113001B (Makarov & Fabricius 1999) and vZ 1128 (Wakker et al. 2003), which were used to assess the foreground interstellar absorption in the direction of FK Com. Comparison star 31 Com is located almost exactly at the north Galactic pole (NGP); FK Com and HD 113001B are on a line through the NGP 10° to either side of 31 Com. FK Com and HD 113001B are at similar *Hipparcos* distances, ~230 pc, while 31 Com is much closer, ~90 pc. The halo star vZ 1128 is only 5° away from FK Com on the sky but lies at a much greater distance, 10 kpc above the plane of the Galaxy. Since the three more distant objects are beyond the bulk of the Galactic disk, their interstellar absorptions should be similar, built up mainly in the first 200 pc or so. The COLDEN tool of the *Chandra* Science Center, based on radio surveys of neutral hydrogen emission, reports $N_{\rm H} \sim 1 \times 10^{20}$ cm^{-2} for the three distant stars and about half that value for the direction of 31 Com. However, the latter object is well inside the Galactic disk, in fact apparently at the edge of a warm bubble that extends to the solar vicinity, and direct measurements indicate a much smaller interstellar column, $N_{\rm H} \sim 1 \times 10^{18}$ cm^{-2} (Piskunov et al. 1997). The importance of accurately identifying the pattern of FUV interstellar absorptions is that they can serve as velocity fiducials to pin down the sometimes uncertain wavelength zero points of *FUSE* spectra.

2.1. *Previous Work*

Unlike some prototypes of a class, which later unceremoniously are rejected as true members, FK Com has long reigned as the most extreme of the FK Com stars.

In the visible, FK Com displays peculiar, variable Hα profiles that are centrally reversed, unusually broad (FWHM ~ 400 km s^{-1}; e.g., Walter & Basri 1982), and whose emission peaks are modulated in synchrony with the rotation period for weeks at a time (Welty et al. 1993; H93). These authors have proposed that the Hα behavior is due to pockets of cool gas suspended quasi-statically in the high corona, $\sim 1 R_\star$ above the surface, analogous to the "prominences" seen associated with magnetic active regions on the Sun (harking back to Merrill's original ideas). Systematic velocity shifts in phase with the spin period would come about from a persistent hemispheric asymmetry in the activity patches lasting for many rotations (Welty et al. 1993).

Solar prominences are the result of twisted and braided magnetic force lines rising above topologically complex active regions (Tandberg-Hanssen 1995). Although superficially long lived, the quasi-stability of the structures belies a highly dynamic internal nature (Zirker et al. 1998). Occasionally, the delicate equilibrium state is disrupted, and prominence material is hurled violently out of the low corona in the form of a mass ejection (Webb et al. 1994).

Optical Doppler imaging demonstrates that FK Com is heavily spotted (e.g., Korhonen et al. 2000), and decades-long photometric time series have revealed that the umbral activity is concentrated at two long-lived active longitudes that are cyclically populated (Jetsu et al. 1993; Korhonen et al. 2002). Large starspots and their quasi-repetitive behavior point to operation of a solar-type dynamo, albeit an extreme case. This is good evidence that, regardless of its origins, hyperactive FK Com is in the early stages of the enigmatic rapid braking phase.

FK Com has been observed extensively in the 1150–3000 Å ultraviolet region by the *International Ultraviolet Explorer* (*IUE*; see, e.g., H93), but unfortunately not by either of the *Hubble Space Telescope* (*HST*) spectrometers, the Goddard High Resolution Spectrograph (GHRS) or the Space Telescope Imaging Spectrograph (STIS). H93 described *IUE* observations of FK Com in spring 1989, coordinated with ground-based spectroscopy and

TABLE 2
FUSE Data Sets

Target	Data Set	t_{exp} (ks)	UT Start Time	Aperture	v_{corr} (km s^{-1})
FK Com	D0750101	12.93	2004 Feb 12.98	LWRS	(+11, +11)
31 Com	P1180401	12.92	2001 Apr 20.78	LWRS	(+20, ...)
HD 113001B	P3020301	5.87	2004 Mar 24.33	MDRS	(+15, +5)
vZ 1128	P1014101	9.15	2000 Jun 18.06	LWRS	(+45, +5)
	P1014102	8.25	2000 Jun 19.86	LWRS	...
	P1014103	15.61	2000 Jun 22.02	LWRS	...

Note.—LWRS = $30'' \times 30''$; MDRS = $4'' \times 20''$; for v_{corr}, the first value is for $\lambda < 1000$ Å, the second for $\lambda > 1000$ Å.

visual photometry. The authors found that the Mg II $\lambda\lambda$2796 ("*k*"), 2803 ("*h*") flux, recorded at ~10 Å resolution in the long-wavelength (LW: 2000–3200 Å) low-dispersion mode, was correlated with the Hα emission, which in turn exhibited significant rotational modulations of its profile shape. On the other hand, the higher temperature C IV feature, recorded at 6 Å resolution in the short-wavelength (SW: 1150–2000 Å) low-dispersion mode, did not appear to correlate with Hα at all. Unfortunately, owing to the low dispersion, detailed shapes of the Mg II blend were not available to compare directly with the rotational behavior of contemporaneous Hα. Earlier, Bianchi et al. (1985) had discussed correlations of *IUE* low-dispersion SW and LW fluxes of FK Com with optical photometry, finding some evidence for a phase dependence. However, again, no detailed profile comparisons were possible. A new appraisal of the existing LW echelle material, to derive representative high-resolution Mg II profiles, is presented in § 2.3.

FK Com has been a frequent target of historical and contemporary X-ray missions and is considered one of the most active of the coronal stars (e.g., Welty & Ramsey 1994; A98). Recent X-ray work includes the *Chandra* High Energy Transmission Grating Spectrometer (HETGS; Buzasi et al. 2003) and *XMM-Newton* (Gondoin et al. 2002). The 42 ks HETGS spectrum was hot ($T \sim 10^7$ K), showing mainly the Lyα lines of hydrogen-like Mg, Ne, and O, with the first 20 ks dominated by a flare. The longer (~63 ks) *XMM-Newton* observation consisted of two similar-length pointings about 2 weeks apart. The first light curve showed a strong flare rise during the initial 15 ks, then flattened for the remaining 15 ks. The second pointing caught a small flare about 5 ks after the start, lasting about 10 ks, followed by 20 ks of relative quiescence, with a mean flux level similar to that at the beginning of the first pointing. In both cases, the EPIC pn CCD-resolution ($R \equiv E/\Delta E \sim 50$) energy distribution was very hot, including prominent 6.5 keV Fe K emission.

Welty & Ramsey (1994) found that successive *Röntgensatellit* (*ROSAT*) PSPC pulse-height spectra were best matched using N_H values that mainly were much smaller than the nominal Galactic column $\sim 1 \times 10^{20}$ cm^{-2} but attained that level during one of the segments, suggesting that the neutral column itself was changing, thus implying a local origin for at least some of the soft absorption. Although the evidence is slim, this is consistent with the idea that high-altitude cool prominence-like material occasionally can partially obscure underlying hot coronal regions (H93). In their modeling of the two *XMM-Newton* pointings on FK Com, Gondoin et al. (2002) simply fixed N_H at 1.3×10^{20} cm^{-2} and did not explore possible short-term variability of the soft absorption. However, the authors did note that the EPIC CCD spectrum became harder as it intensified, contrary to the softening expected when the absorber thins out (H93). However, given the flarelike character of the main spectral changes in the *XMM-Newton* light curves and the limited duration of the pointings, an absorption mechanism operating at other times cannot be excluded.

2.2. *Far Ultraviolet Spectroscopic Explorer*

The *FUSE* mission and the in-flight performance of its instrument package have been documented by Moos et al. (2000) and Sahnow et al. (2000). The spectral resolution achieved with the large science aperture (LWRS) used in the FK Com program is $R \equiv \lambda/\Delta\lambda \sim 2 \times 10^4$, fully adequate to resolve the stellar features given the anticipated large rotational broadening.

The *FUSE* pointing on FK Com commenced 23:36 UT, 2004 February 12, with a nominal exposure of 13 ks. The observation covered parts of six *FUSE* orbits and, from start to finish, 8.5 hr of clock time (15% in rotational phase: $\phi = 0.58-0.73$ in the ephemeris of Jetsu et al. 1993). Table 2 presents a catalog of the *FUSE* observations of FK Com, comparison star 31 Com, and a summary of pointings on the two sdO stars mentioned above, whose interstellar medium (ISM) absorption content was assessed for the program. The table includes empirical velocity corrections to bring the pipeline processed spectra into the heliocentric reference frame, separated if warranted into two wavelength regions (thermally driven channel misalignments can impose different systematic wavelength shifts on different spectral segments). For the stars other than FK Com, these corrections were obtained by adjusting the centroids of apparent stellar features to the radial velocity of the object. For FK Com, the offset was derived by matching interstellar absorption dips to the velocity of ISM features in better calibrated *IUE* echelle spectra of the Mg II doublet (as described in § 2.4).

The FK Com FUV data sets were retrieved from the Multimission Archive at Space Telescope (MAST) and recalibrated with CalFUSE version 3.1[2] using the default "event burst" and background correction options. The individual subexposures were screened for orbital day and night: during the daylight portions of the orbit, stellar features like C III λ977 can be affected by scattered solar radiation in the SiC channels, and airglow emissions of atomic hydrogen and oxygen are much stronger in all of the channels as well. Of the total exposure, 5.6 ks was on the day side, and 7.8 ks was on the night side. In general appearance, the eight independent background-subtracted detector segments contain a series of isolated broad emission lines with little evidence of a stellar continuum.

[2] The CalFUSE Pipeline Reference Guide Version 1.3 (maintained by V. Dixon, J. Kruk, and E. Murphy; http://fuse.pha.jhu.edu/analysis/pipeline_reference.html).

The O VI $\lambda\lambda$1031, 1037 doublet (at $T \sim 3 \times 10^5$ K, hottest of the bright resonance lines in FUV spectra of late-type stars) normally appears in four detector segments: LiF 1A, LiF 2B, SiC 1A, and SiC 2B. In the observation of FK Com, however, no stellar signal was obvious in SiC 1A. (Thermal flexing of the instrument occasionally causes the stellar image in one of the nonguiding channels [the Fine Error Sensor was tracking through the LiF 1 telescope] to drift outside the $30'' \times 30''$ LWRS aperture.) Of the remaining three channels, LiF 1A has the best signal (corresponding to signal-to-noise ratio [S/N] of $\sim$10 per 50 mÅ resolution element at peak of λ1031), followed closely by LiF 2B, with SiC 2B at about half the strength of the other two. Ordinarily it is recommended to analyze the independent detector segments separately, owing to the differences in sensitivity, resolution, and sampling.[3] However, the FK Com spectrum is underexposed (unfortunately, only a fraction of the originally requested exposure time was approved by the Telescope Allocation Committee) and the features are very broad, so it was felt that co-addition of the separate O VI channels was warranted. In the region longward of $\sim$1100 Å (which contains the C III multiplet near 1175 Å), the LiF 2A and 1B segments both had peak S/N of $\sim$6 per resolution element and thus also were suitable for co-addition. For C III λ977, on the other hand, stellar counts were present only in the SiC 2A channel (corresponding to peak S/N of $\sim$7 per 50 mÅ resolution element), with nothing obvious, except airglow, in companion SiC 1B, precluding co-addition.

Before merging the eight partially overlapping detector segments, the up to six channel-specific subexposures (each representing the unocculted part of a *FUSE* orbit) were co-added. To accomplish this, the individual exposures were aligned to the wavelength scale of the first in the series by cross-correlation (of dominant stellar features, e.g., O VI λ1031 or C III λ977), the adjusted spectrum was interpolated onto a reference linear wavelength scale with uniform 6 mÅ sampling, and then the spectra were co-added to form an average of higher S/N. If the target was present in some of the exposures but not others, only the on-source intervals were included.

Finally, the independent partially overlapping detector segments that contained useful signals were merged. As for the subexposures, the full segments were aligned by cross-correlation of bright features in common, as interpolated onto a reference wavelength scale (e.g., LiF 1A for O VI), and the overlapping intervals were co-added, weighted according to their integrated counts (in a prominent reference feature, say, O VI). A weighted average of the photometric error (assigned by the pipeline processing) was retained, together with the standard deviation of the fluxes. The latter is an empirical gauge of the local flux errors and includes such effects as "fixed pattern" noise (due to incomplete flat-fielding) in addition to the normal photon statistics component.

The *FUSE* spectra of HD 113001B and vZ 1128 were treated similarly. The sdO exposures generally had high S/N to aid the cross-correlation alignments, and usually all the channels had at least some signal, so a more thorough merging of the partially redundant detector segments was possible. In the comparisons shown later (Fig. 5), nighttime-only spectra were used for the C III λ977 region, but night+day fluxes for the LiF-dominated intervals (such as O VI λ1031).

The concatenated *FUSE* spectrum of FK Com is illustrated in Figure 1. The fluxes were not corrected for extinction because the appropriate A_V is uncertain, especially given that part of the absorption might be local (and highly variable) rather than truly interstellar. Even on the compressed wavelength scale, the stellar emission features are distinctly broad. The O VI doublet, C III λ977 resonance line, and λ1175 multiplet all are strong; broad He II Baγ emission at 1084 Å is less prominent (and mixed with narrow N II λ1085 airglow lines in the dayside spectrum) but possibly present, and there are suggestions of additional He II features at shorter wavelengths (blended with H I Lyβ in the case of He II Baδ at 1026 Å). Finally, a weak "continuum" appears between 1110 and 1140 Å. This very likely represents a forest of fluoresced Fe II transitions, pumped by broad H I Lyα, originally identified in *FUSE* spectra of the late-type supergiant α TrA and the intermediate-mass pre–main-sequence star HD 104237 by Harper et al. (2001) and seen also in Herbig Ae stars such as HD 163296 (Deleuil et al. 2005).

Table 3 summarizes measurements of the prominent lines: C III λ977, the O VI doublet, and the C III λ1175 multiplet. Line centroids and FWHMs were estimated by fitting Gaussians to the (in some cases) complex profiles after smoothing with a 25 bin FWHM Gaussian (0.15 Å $\sim$ 45 km s^{-1}, about three resolution elements) to improve characterization of apparent absorption structure, which was ignored in the modeling to the extent possible. As such, the derived Gaussian parameters are less certain than the formal statistical errors (based on Lenz & Ayres 1992). Line fluxes were determined by integration of the intensities in a wavelength band of 5–7 Å, depending on the feature, including any apparent absorption structure. In the case of O VI λ1031, two independent multiple-Gaussian models were derived: these are described in more detail in § 3.2.

2.3. *International Ultraviolet Explorer*

The MAST lists 123 large-aperture *IUE* observations of FK Com, 99 of which are split nearly equally between low-dispersion ($R \sim 300$) SW and LW exposures. The remaining observations are high dispersion ($R \sim 1 \times 10^4$): 23 LW, and a single (very weakly exposed) SW spectrum. Of the former, 15 were 5 ks, or longer, in duration and well exposed (or saturated, in some cases) at the important Mg II λ2800 chromospheric emission doublet.

In the present study, the set of 15 well-exposed LW echellegrams of FK Com constituted a sample of representative Mg II line shapes to compare with the FUV emissions recorded at similar resolution by *FUSE*. Exposures from both LW cameras (LWP and LWR, which were active at different times during the mission) were utilized, covering the period 1981–1991. Only spectra that were unsaturated at the peaks of Mg II *k* and *h* ultimately were combined into average profiles, although the centroids of the Mg II absorption dips (likely interstellar) were measured in the deeper exposures, as long as the bottom portion of the dip was not overexposed. Table 4 provides a catalog of the *IUE* exposures.

Based on the 15 echellegrams used for this purpose, and averaging the results for the *k* and *h* components, the Mg II absorption velocity was -17 ± 5 km s^{-1}. The uncertainty is one standard deviation, illustrating the typical displacement of a single measurement from the mean, comparable to the nominal wavelength zero-point error of LW-HI echellegrams.[4] If the deviations truly are random, representing, say, uncorrelated systematic errors or simple photometric uncertainties, then in principle the precision of the average would improve to $\sim$1 km s^{-1}. The Mg II absorption velocity is 7 km s^{-1} redward of the stellar

[3] *FUSE* Data Analysis Cookbook Version 3 (maintained by R. Sankrit and B.-G. Andersson; http://fuse.pha.jhu.edu/analysis/cookbook.html).

[4] A Study of the Wavelength Calibration of NEWSIPS High-Dispersion Spectra, by Myron A. Smith (http://archive.stsci.edu/iue/newsips/wavestudy).

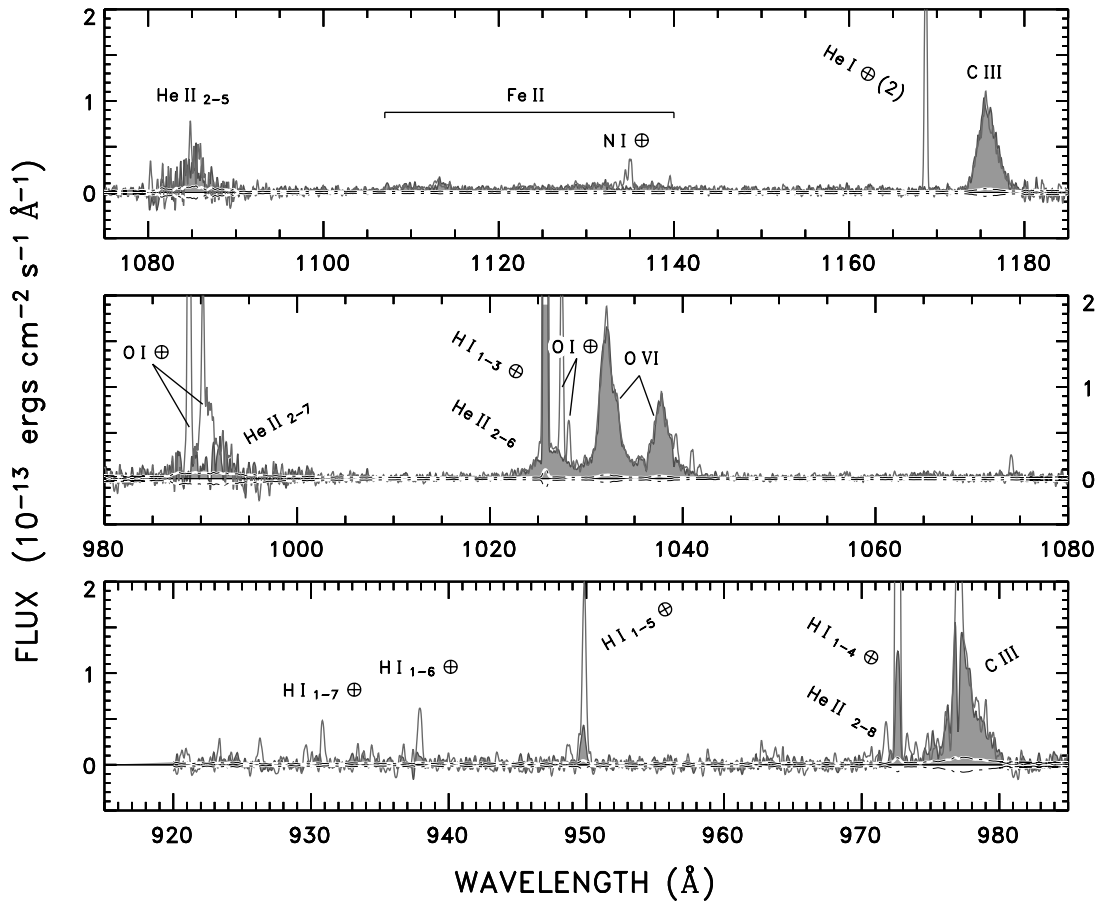

FIG. 1.—Overview of *FUSE* spectrum of FK Com. Shading indicates nighttime observation; the thin line is daytime, highlighting terrestrial airglow features (*circled plus sign*). Second-order He II λ584 airglow emission appears at 1168 Å. No correction for extinction was applied. The dot-dashed line is the estimated $\pm 1\ \sigma$ noise level for the smoothed nighttime spectrum (25 bin [0.15 Å $\sim$ 45 km s^{-1}] FWHM Gaussian filter). [*See the electronic edition of the Journal for a color version of this figure*.]

radial velocity and 13 km s^{-1} blueward of the (much weaker) ISM feature recorded in 31 Com by *HST* GHRS (-4 km s^{-1}; Piskunov et al. 1997).

Even though the Mg II lines are separated by a healthy 770 km s^{-1}, they are partially blended by the extreme broadening in the FK Com spectrum, so that the red wing of *k* is strongly affected by the blue wing of *h*, and vice versa. For the purpose of comparison, a hybrid Mg II profile was constructed by joining the blue wing of *k* to the red wing of *h*, the latter suitably scaled (by a factor of 1.2) so that the peak of *h* matched that of *k*. The hybrid profile should more fairly represent the true line shape of an isolated feature having the same general opacity properties as one of the Mg II components. Figure 2 illustrates the hybridization procedure schematically.

The Mg II lines of FK Com in the existing *IUE* collection exhibit considerable variability as a consequence of phase modulations and, in at least one case, a large flare. Subsets of the hybrid profiles were separately combined to represent the "red-asymmetry" and "blue-asymmetry" extremes of the line shape behavior, as noted in Table 4.

TABLE 3
FUSE MEASUREMENTS

Transition	Δv (km s^{-1})	FWHM (km s^{-1})	$f_{\rm tot}$ ($\lambda_0 \rightarrow \lambda_1$)	f_C	Notes
C III 977.020	+63 ± 6	510 ± 13	2.3 ± 0.2 (974.5–980.5)	0.1	Night
O VI 1031.926	+90 ± 2	530 ± 5	2.9 ± 0.1 (1030.0–1035.0)	0.1	Both
Narrow component (1)	+40	310	27%	0.00	
Broad component (1)	+160	810	73%	0.00	
Narrow component (2)	+6	310	34%	0.15	
Broad component (2)	+185	570	66%	0.15	
O VI 1037.617	+60 ± 7	480 ± 8	1.4 ± 0.1 (1035.5–1040.5)	0.1	Night
C III 1175.711	...	645 ± 7	2.5 ± 0.1 (1172.5–1179.5)	0.0	Both

NOTES.—Integrated flux, $f_{\rm tot}$ (above pseudocontinuum level), is in 10^{-13} ergs cm^{-2} s^{-1}, with integration limits λ_0 to λ_1 (Å); pseudocontinuum flux density, f_C, is in 10^{-13} ergs cm^{-2} s^{-1} Å^{-1}; no correction for extinction. In Notes column, "Night" = nighttime-only spectrum; "Both" = night+day.

TABLE 4
IUE LW-HI Spectra

Image Number	t_{exp} (ks)	UT Start Time	Notes
LWR 09633	5.4	1981 Jan 04.82	Large flare
LWR 13065	7.2	1982 Apr 22.60	Blue*
LWR 13069	7.2	1982 Apr 23.59	Red*
LWR 13077	7.2	1982 Apr 25.58	Blue*
LWR 16546	5.4	1983 Aug 08.11	Blue*
LWR 16558	9.0	1983 Aug 09.63	Red*
LWP 05047	16.2	1984 Dec 20.75	Red (sat)
LWP 05054	18.0	1984 Dec 21.74	Blue (sat)
LWP 05056	5.1	1984 Dec 22.17	Blue*
LWP 05059	18.9	1984 Dec 22.75	Blue (sat)
LWP 05060	8.4	1984 Dec 23.17	Red*
LWP 05065	19.8	1984 Dec 23.75	Red (sat)
LWP 05071	19.8	1984 Dec 24.74	Blue (sat)
LWP 05072	7.2	1984 Dec 25.18	Red*
LWP 19468	7.8	1990 Dec 24.41	Red*

Notes.—In Notes column, "Red" = red-asymmetric line shape, "Blue" = blue-asymmetric, "sat" = overexposed. Data sets followed by asterisks were co-added into the reference profile for that asymmetry class.

2.4. *FUV Line Shapes versus* Mg II

The C III λ977, O VI doublet, and Mg II *kh* hybrid features of FK Com are compared in Figure 3. The FUV profiles were smoothed, as in Figure 1, for display purposes. The *IUE kh* hybrid profiles are depicted at similar resolution, scaled down in flux density to match the general level of the FUV features. The deep central reversal in Mg II very likely is interstellar. The analogous central reversal in C III λ977, likely also interstellar, falls at -6 ± 1 km s^{-1} (with respect to the pipeline processed wavelength scale), similar to the ISM velocity toward 31 Com mentioned previously, but 11 km s^{-1} redward of the Mg II velocity determined from *IUE*. Given the probable more accurate velocity calibration of the *IUE* material, a correction of 11 km s^{-1} was applied to the C III region (and O VI as well), to align the central dip of λ977 with that of the average *kh* profile. The spectra illustrated in Figure 3 are in the velocity frame of FK Com, and a "pseudocontinuum" flux density of 0.1×10^{-13} ergs cm^{-2} s^{-1} Å^{-1} was subtracted from the C III and O VI features according to the appearance of the surrounding spectrum; moreover, an analogous baseline level was removed from the *kh* composite profiles. (The FUV baselines are not true continuum, since they are not spectrally pervasive, but rather appear to be very broad, faint intrinsic components of the bright lines, perhaps partly instrumental scattered light.) There are a number of striking aspects to the comparison.

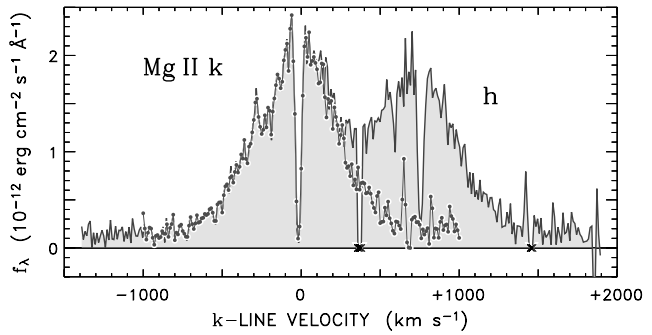

Fig. 2.—Construction of "hybrid" Mg II *kh* profile from archival *IUE* LW echelle spectrum. Shading displays the Mg II region of FK Com, on a heliocentric velocity scale referenced to the λ2796.352 "*k*" line; from LWR 09633, a 1.5 hr exposure was taken on 1981 January 4. This is perhaps an extreme example of the mutual blending of *k* and *h*, since at the time FK Com was in flare outburst and Mg II was about twice its quiescent flux. Sharp dips near centers of Mg II components are interstellar; other dropouts marked with crosses are camera artifacts flagged by the *IUE* pipeline. Narrow emission spikes usually are cosmic-ray "hits." Darker connected dots represent the hybrid profile, designed to mimic a single Mg II component free of mutual blending effects. It is built from the blue side of *k* and the red side of *h*; the latter is scaled upward by a factor of 1.2 to account for difference in line strengths. [*See the electronic edition of the Journal for a color version of this figure.*]

First, the C III and O VI profiles are remarkably broad, with FWHM in excess of 500 km s^{-1}. This is about twice as wide as the previous record holders among the normal late-type stars, fast rotating G0 III Hertzsprung gap giants such as 31 Com (as illustrated in § 3.2; see also A98). Curiously, fast spinning Herbig Ae stars also can display extremely broad, redshifted O VI profiles as described by Roberge et al. (2001) for the case of AB Aurigae (FWHM $\sim$ 400 km s^{-1}, $v \sim +100$ km s^{-1}). For the Herbig star HD 163296, mentioned earlier, Deleuil et al. (2005) attributed the broad, complex line shapes of O VI and C III to a corotating ring or disk of $\sim 10^5$ K gas, arising from magnetospheric accretion or a wind collision zone forced by a global magnetic dipole, qualitatively matching Merrill's original suggestion for FK Com.

Second, the FUV profiles are noticeably asymmetric with respect to the zero point of the stellar reference frame, showing either a steep, possibly absorbed, blue wing or an extended flatter red wing, depending on one's prejudices. At the same time, the C III and O VI line shapes are very similar to one another and very close to the average Mg II *kh* red-asymmetry profile, aside from a prominent blueward absorption in C III.

Third, the O VI λ1037 feature, when scaled up by the optically thin flux ratio 2 : 1 (Fig. 3, *bottom panel*), is nearly identical to its stronger λ1031 partner, except for narrow absorptions near -400 and +400 km s^{-1}. Both O VI line shapes show slightly redshifted narrow central dips, although their significance is low. The weak blueward enhancement of λ1037 possibly is due to a pair of C II lines ($\lambda\lambda$1036.34, 1037.02), which often are seen in emission in late-type giant spectra (Dupree et al. 2005), usually much weaker than O VI. The close similarity of the blue wings of λ1031 and scaled λ1037 argues against an absorption scenario in which the red asymmetry is produced by, say, a 10^5 K outflow. (The factor of 2 larger oscillator strength of λ1031 should produce twice as large relative absorption in its own profile compared with its weaker partner.)

Further details concerning these profile characteristics are discussed in § 3.

2.5. *Doppler Imaging in the Visible*

High-resolution ($R \sim 3 \times 10^4$) spectra of FK Com in the visible were collected at the Nordic Optical Telescope (NOT, La Palma, Spain) with its SOFIN echelle spectrograph. Sixteen exposures were taken during 10 nights between 2004 January 30 and February 11, immediately prior to the *FUSE* pointing. Sequential observations from the same night, recorded within the phase smearing limit ($\Delta\phi \lesssim 0.01$) of about 40 minutes, were combined to increase S/N. Data reductions were done with the "4A" package described by Ilyin (2000).

The "Doppler Imaging" inversion technique (see, e.g., Vogt & Penrod 1983), exploiting Tikhonov regularization (Piskunov et al. 1990), was applied to the high-resolution visible spectra to derive a surface temperature map of FK Com for the epoch of the *FUSE* program. Full details of the inversion procedure, stellar parameters, and code are provided in Korhonen et al. (2000).

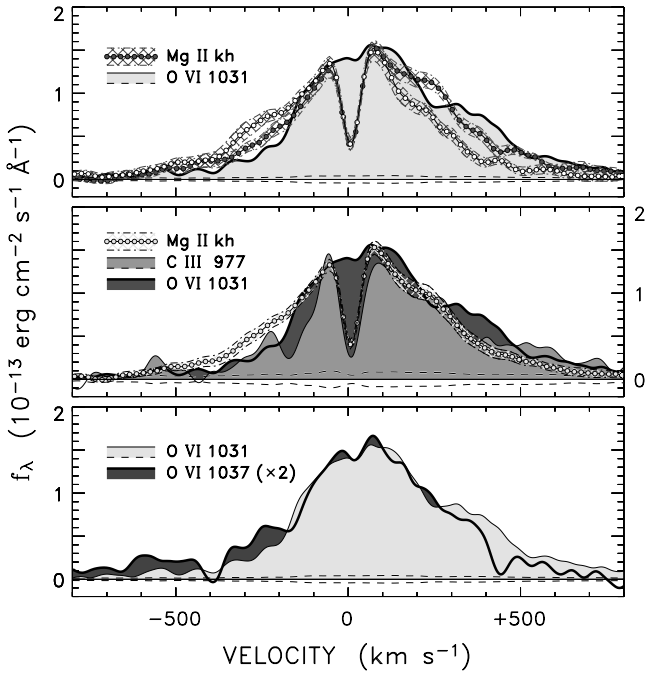

FIG. 3.—Comparison of prominent FUV emission features of FK Com, including hybrid Mg II *kh* profiles. In the top panel, the shaded line shape is *FUSE* O VI λ1031, while dotted/dashed lines are for two separate Mg II *kh* co-additions: one for predominantly red-asymmetric profiles, the other for predominantly blue-asymmetric. Cross-hatching indicates standard error of the mean of the typically five independent observations in each average. The Mg II *kh* profiles were scaled down in flux density to match the FUV lines. The middle panel compares C III λ977, O VI λ1031, and Mg II *kh*, the latter based on the average of well-exposed *IUE* profiles regardless of asymmetry type (but excluding the one large flare). The bottom panel compares the O VI components, scaling the weaker (λ1037) upward by the optically thin ratio 2 : 1. The FUV profiles were adjusted in velocity to match interstellar absorptions, and a pseudocontinuum of 0.1×10^{-13} ergs cm^{-2} s^{-1} Å^{-1} was subtracted from each (prior to scaling, in the case of λ1037). Note the blueward dip in C III λ977 near -180 km s^{-1} (*middle panel*) and absorptions that flank O VI λ1037 at $\pm$400 km s^{-1} (*bottom panel*). Dashed lines indicate ± 1 σ photometric errors, taking into account the 25 bin smoothing, for O VI λ1031 in the top and bottom panels and for C III λ977 in the middle panel. C III and O VI λ1037 are from a nighttime-only spectrum. [*See the electronic edition of the Journal for a color version of this figure*.]

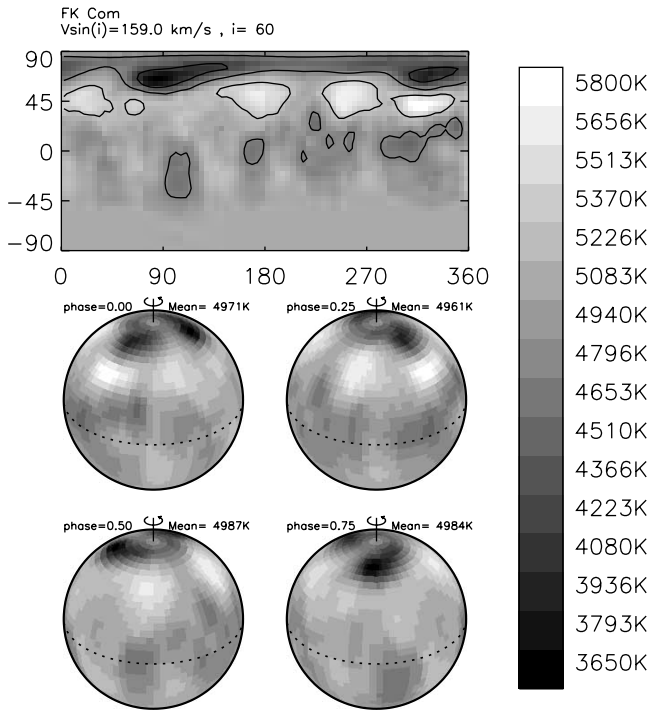

FIG. 4.—Doppler image of FK Com for 2004 February epoch of *FUSE* observation. In the pseudo-Mercator projection (*top*), longitude 0° is at the substellar point at $\phi = 0$, longitude 270° is at the substellar point at $\phi = 0.25$, and so forth. Hemispheric temperature maps displayed at the bottom are from four phase orientations 90° apart, with inclination of 60°. The bar at the right indicates surface temperature (in K). Phases covered by *FUSE* pointing were $\phi = 0.58-0.73$, i.e., the bottom two hemispheric maps.

Figure 4 depicts the 2004 February surface map of FK Com. It shows two main high-latitude starspots: a cooler one located at average longitude 80° and a second, of slightly lower contrast, trailing by about 130°, consistent with the earlier detected "permanent" active longitudes (Jetsu et al. 1993; Korhonen et al. 2002).

3. ANALYSIS

3.1. *The Blueward Absorption Component in* C III λ977

Initially we thought that the conspicuous blueward absorption in C III λ977 might result from a $\sim 8 \times 10^4$ K outflow (cooler than, say, the 10^6 K coronal wind of the Sun, or the $\sim 10^7$ K X-ray temperature of FK Com itself), as has been proposed to explain asymmetric FUV profiles of other giant stars (Dupree et al. 2005), or a transient dip due to a prominence-like structure rotating into view, as occasionally is seen in Hα time series. For good measure, however, we entertained the possibility of absorption by some species other than C III, perhaps interstellar.

Figure 5 compares selected FK Com emission features to the two sdO absorption spectra, in the heliocentric reference frame, with prominent ISM features highlighted. The spectra of the two subdwarfs were adjusted in velocity to place their photospheric features (mainly N IV, S IV, and S VI) at the respective stellar radial velocities (see Table 1), which should then align any interstellar features at whatever peculiar velocity they share in that direction. That apparent ISM velocity is -25 ± 3 km s^{-1} (based mainly on O I and N I), somewhat shortward of the directly measured Mg II absorption velocity in FK Com. One sees in the C III λ977 panel that a blueward absorption is present in both sdO stars in addition to ISM C III. One possibility is H_2, as suggested by Dupree et al. (2005) in the case of the yellow supergiant β Draconis. However, a series of stronger H_2 absorptions in the O VI region, such as seen in AB Aur (Roberge et al. 2001), are not present in the FK Com spectrum. A more likely identification is O I λ976.448, particularly since a companion O I line, λ1039.230, possibly is present in the red wing of O VI λ1037. The blueward absorption component in O VI λ1037 likely is due to interstellar C II λ1036.337, another ground-state transition.

In the C III λ1175 multiplet panel, no prominent interstellar absorptions are apparent (certainly not from C III itself, since the λ1175 complex arises from highly excited levels). The individual C III multiplet components can be seen in the velocity-separated hot-star absorptions but are fused into a single profile in the highly broadened FK Com spectrum.

The conclusion is that the blueward absorption component in C III λ977 simply represents intervening interstellar gas, rather than something more exotic like a warm wind from the star or prominence material in the line of sight. This urges caution in the interpretation of asymmetric C III profiles in *FUSE* spectra of similarly distant objects, such as the G-type supergiants, for which interstellar O I absorption (or O I in a slow cool wind) could masquerade as a fast outflow at C III temperatures.

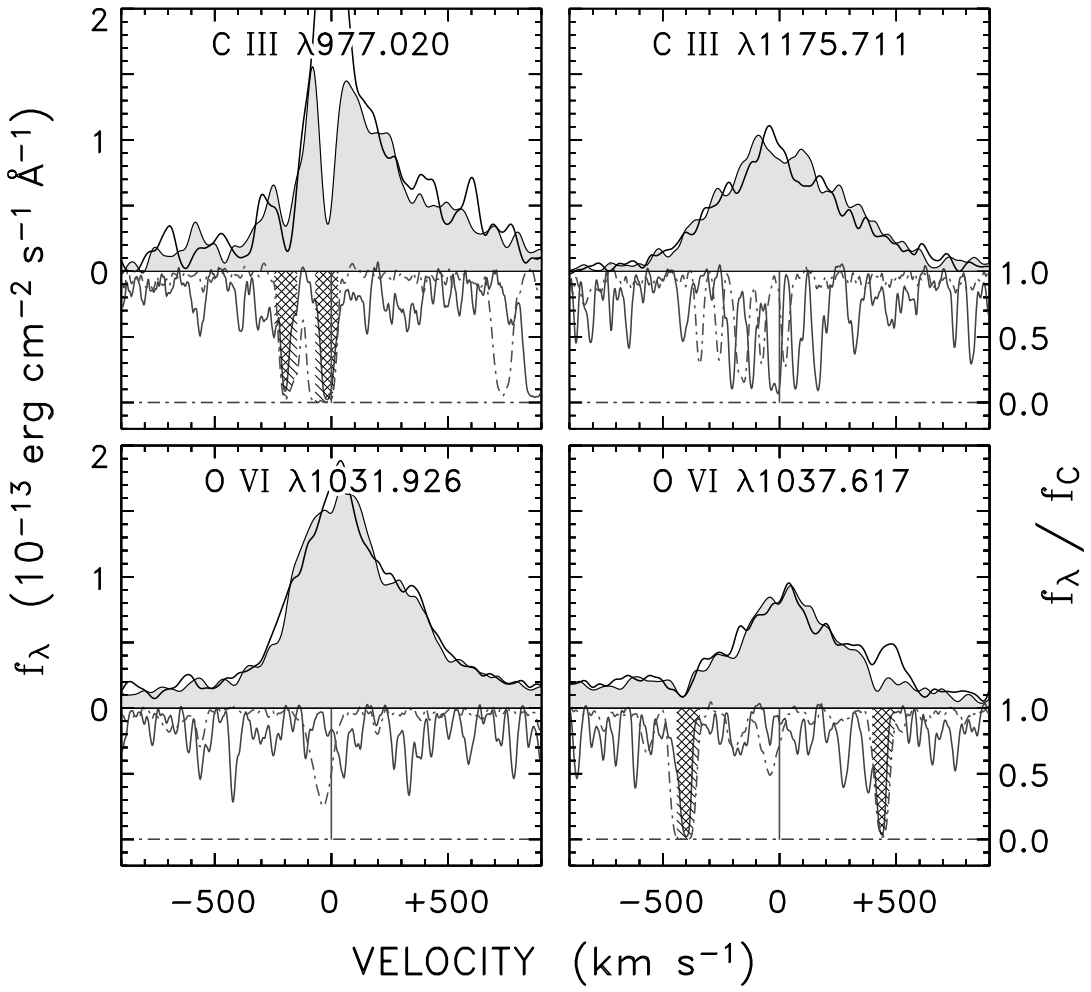

FIG. 5.—Comparison of FK Com hot-line emission profiles (*shaded*: nighttime; *thin solid*: daytime) with interstellar absorption spectra of two sdO stars (*solid line:* HD 113001B; *dot-dashed line*: vZ 1128), in the heliocentric velocity frame. Cross-hatching in the lower half of each panel indicates strong ISM absorptions in common with the subdwarfs. Note the blueshifted O VI λ1031 dip exclusively in the spectrum of vZ 1128 ($d \sim 10$ kpc), representing infalling hot halo gas (Wakker et al. 2003). HD 113001B is much closer (220 pc, about the distance of FK Com) and lacks any O VI in its foreground. Absorption structure in the lower part of the C III λ1175 panel is entirely stellar, although muddled by the large radial velocity separation (140 km s^{-1}) of the two subdwarfs. In the O VI λ1037 panel, ISM absorption near −400 km s^{-1} is C II λ1036.337, while that near +400 km s^{-1} is O I λ1039.230 (note the "hump" in the daytime line, probably airglow). In the λ977 panel, the central dip is interstellar C III λ977.020, while the blueward feature likely is interstellar O I λ976.448. [*See the electronic edition of the Journal for a color version of this figure.*]

3.2. *Superrotational Broadening versus Multiple-Gaussian Decomposition*

The C III and O VI emissions of FK Com are remarkably broad, certainly greatly in excess of the ∼280 km s^{-1} FWHM expected solely from the photospheric $v \sin i$. The "superrotational" broadening of hot lines in normal Hertzsprung gap giants was documented by A98 and attributed to highly extended emission zones, reaching out to as much as a stellar radius above the photosphere. An example is illustrated in Figure 6, for the comparison star 31 Com. The underlying line shape represents a co-addition of *HST* STIS profiles of the resonance doublets Si IV, C IV, and N V, which form over the temperature range 6×10^4–2×10^5 K, overlapping the range spanned by C III and O VI. Also shown is the *FUSE* O VI λ1031 profile, scaled to the STIS hot-line average (in flux and velocity). The excellent agreement between *FUSE* and STIS is typical of active giant stars and demonstrates that all of the hot-line profiles are essentially identical in shape (when local distortions due to, say, blends are accounted for; see, e.g., Ayres 2006). The smaller darker profile is a similar co-addition of low-excitation chromospheric emissions, such as C I and O I, from STIS, and displays the flat-topped character of extreme photospheric rotational broadening.

The composite hot-line profile of 31 Com has a roughly Gaussian shape and, if modeled in that way, yields FWHM ∼ 190 km s^{-1}, nearly twice as wide as anticipated from the photospheric $v \sin i$ (FWHM ∼ 100 km s^{-1}). Alternatively, the composite profile can be decomposed into a sum of "narrow" and "broad" components (see, e.g., Wood et al. 1997). In this example, the narrow component has FWHM ∼ 154 km s^{-1} (50% superrotation), is slightly redshifted (+4 km s^{-1}), and accounts for a little more than half of the total flux. The broad component has an FWHM twice as large (345 km s^{-1}), is slightly blueshifted (−7 km s^{-1}), and accounts for the other half of the total flux.

The prevailing interpretation of the double-Gaussian decomposition is that the two components represent different general classes of active structures in the stellar outer atmosphere: steady heating (narrow components) and highly dynamic (broad), the latter in analogy with "transition zone explosive events" seen commonly on the Sun in the magnetic supergranulation "network" (Wood et al. 1997).

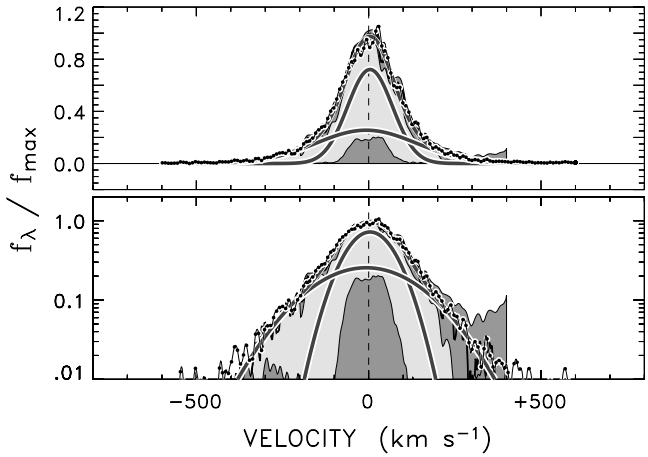

FIG. 6.—Double-Gaussian decomposition of average hot-line profile of Hertzsprung gap giant 31 Com (linear scale in top panel, logarithmic in bottom panel). The light shaded line shape is the filtered average of Si IV, C IV, and N V doublets from *HST* STIS medium-resolution ($R \sim 4 \times 10^4$) echelle spectra; darker shading indicates standard deviation of individual scaled profiles from the mean (with deviant points eliminated). The smaller central flat-topped line shape is the similar average of low-excitation, narrow chromospheric species such as O I and C I, and mirrors expected photospheric rotational profile. Connected dots represent the *FUSE* profile of O VI λ1031, which closely follows the hot-line average. The lower two smooth lines are "narrow" and "broad" components of double-Gaussian decomposition. The sum is the upper line running closely through the STIS profile (and *FUSE* O VI). [*See the electronic edition of the Journal for a color version of this figure*.]

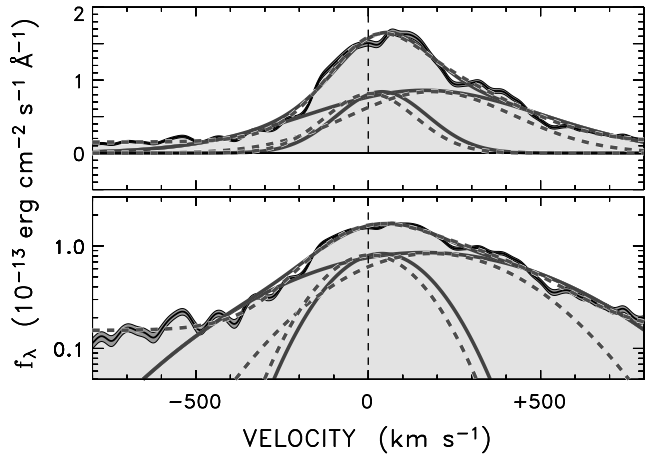

FIG. 7.—Similar to Fig. 6, but for the smoothed O VI λ1031 profile of FK Com. Here darker shading represents standard deviation of the three detector segments merged to form the composite line shape. Two sets of double-Gaussian decompositions are illustrated, for different assumed pseudocontinuum levels (*solid line*: 0.00; *dashed line*: 0.15, in units of the ordinate), bracketing apparent flux density baselines far from line center. Three lines are shown for each decomposition: narrow component, broad component, and sum. For the higher baseline case (*dashed line*), the sum is distinguished from the lower pseudocontinuum case mainly far from line center. Both cases require a strongly redshifted broad component, with a centrally located narrow component. [*See the electronic edition of the Journal for a color version of this figure*.]

Figure 7 illustrates a similar decomposition of the *FUSE* O VI λ1031 profile of FK Com. A single-component Gaussian fit would have an FWHM of about 530 km s^{-1}, with a centroid redshift of +90 km s^{-1}. In the double-Gaussian paradigm, with no compensation for a pseudocontinuum level, the fitted "narrow" component is somewhat less redshifted (+40 km s^{-1}), has FWHM $\sim$ 310 km s^{-1}, and accounts for only one-third of the total flux. The broad component is strongly redshifted (+160 km s^{-1}), has more than twice the FWHM (a remarkable 810 km s^{-1}), and with a 70% contribution dominates the total flux. Unlike 31 Com, the narrow component is close to the expected rotational width.

Increasing the pseudocontinuum "baseline" to 0.15×10^{-13} ergs cm^{-2} s^{-1} Å^{-1} significantly affects the decomposition. The "narrow" component moves closer to line center, at only +6 km s^{-1}, its width remains at 310 km s^{-1}, and its share of the total flux increases slightly although still near one-third. The second component shrinks in width to "only" 570 km s^{-1}, its redshift increases to 185 km s^{-1}, and it still accounts for two-thirds of the total flux. Given the low S/N of the O VI profile and the uncertainty as to the origin and appropriate amplitude of the baseline flux in its vicinity, the two alternative decompositions probably fairly bracket the likely range of possibilities, at least within the two-component paradigm. The conclusion is that the O VI λ1031 line shape can be represented, in the pure emission context, by one component near the stellar velocity and close to the expected rotational width and a second component of about twice the broadening displaced by a redshift comparable to that expected at, or above, the receding limb of the star.

4. DISCUSSION

The *FUSE* spectra of FK Com are tantalizing from the point of view that the evident extreme broadening of the hot lines fully continues the trend seen in normal fast spinning Hertzsprung gap giants, yet the large redward velocity bias of the features is unlike any behavior encountered in normal giants, although curiously it shares similarities with hot-line profiles of Herbig Ae stars, evolutionary precursors to some of the yellow giants.

As we argued previously, on the basis of the joint appearance of the O VI blue wing profiles, the strong redward asymmetry of the hot lines is unlikely to be due to a warm outflow. The existence of nearly identical red asymmetries in a subset of the historical Mg II profiles suggests that the hot-line redshift bias might be specific to the singular *FUSE* observation, rather than a persistent, phase independent phenomenon. A natural underlying cause would be a skewed distribution of activity on the stellar surface. The contemporaneous optical Doppler map suggests that the photospheric active regions were dominantly in the polar regions of the approaching hemisphere, opposite to the expected longitude range to produce a redshifted global emission profile, unless the bright $\sim 10^5$ K structures were *leading* the photospheric spots in phase, and the trailing umbral regions were deficient in O VI emission. The coronal emission structures extending over to the receding hemisphere could be "superrotation broadened," if the warm loops were highly extended in altitude and some were rooted in the midlatitudes. In this situation, there should be a phase modulation of the O VI emission centroid when there is a single large active region on the surface of FK Com, as often is the case. The narrow component could then represent more uniformly distributed compact surface emission regions.

If, instead, one were to assign the broad component to a global population of an exaggerated version of solar explosive events, then one would have to explain the enormous redward bias of O VI in the FK Com observation. No such bias is seen in 31 Com, which, although not as extreme as FK Com, still is at the top of the distribution of observed Hertzsprung gap giants in $L_{\rm C\,IV}/L_{\rm bol}$ and $L_{\rm X}/L_{\rm bol}$, only about an order of magnitude short of FK Com in both measures. One could imagine, nevertheless, that bipolar flows from X-point magnetic reconnection events (e.g., Innes et al. 1997) at high altitudes might develop a velocity centroid bias owing to the asymmetric environment into which the opposing

jets propagate: inward-directed debris encounter systematically higher densities (owing to the hydrostatic stratification or narrowing throats of coronal magnetic "funnels") and release a larger fraction of their internal energy by collisionally excited radiation, whereas outward-directed material might cool mainly by free expansion and thus be less emissive in FUV lines. The difference between this situation and the former (rotational modulation) is that the O VI centroid should be persistently redshifted.

Finally, a redward bias might develop from downflows associated with continual flare activity. For example, downdrafts of up to 400 km s^{-1} have been recorded in postflare arcade systems on the Sun (e.g., Innes & Wang 2004). Here, again, the O VI profile asymmetry might be semipermanent rather than episodic, depending on the relative frequency of the initiating flare events.

Regardless of the origin of the hot-line asymmetries, it is clear that the FK Com corona, at least the thermal regime traced by the FUV lines, is highly complex in supporting very extended emission structures or highly dynamic processes, or both.

In this connection, Jardine & van Ballegooijen (2005) recently proposed a mechanism to explain the presence of "slingshot prominences" at large distances from rapidly rotating dwarf stars, for which independent evidence suggests that the X-ray corona is very compact. The authors' model traps the cool prominence gas in closed magnetic bubbles, reconnecting and condensing out in the tenuous hot stellar wind, rather than in association with extended cool coronal loops rooted in the photosphere (like true prominences on the Sun). In the particular case of FK Com, however, the presence of substantial amounts of warm 3×10^5 K "subcoronal" gas over the full velocity range that Hα and Mg II occupy argues that the lower excitation material is colocated with the main corona proper, rather than existing merely as passive condensates in a massive hot outflow.

5. FOR THE FUTURE

FK Com has lived up to the promise of providing exaggerated high-energy spectral response to its ultrafast rotation and hyperactive corona. Unfortunately, without full coverage of the phases, the existing essentially singular FUV spectrum cannot tame any of the rampant speculation offered to explain the odd spectral properties. Additional progress with *FUSE* is unlikely in the near future because its degraded maneuvering system currently restricts pointings to high-declination objects, not a virtue of FK Com. It would be an ideal target for the *HST* replacement instrument, Cosmic Origins Spectrograph (COS; Green 1998), which could capture the important hot lines (Si IV, C IV, and N V) longward of Lyα, but the fate of the *Hubble* servicing mission to install COS is up in the air, so to speak. *Chandra* HETGS has sufficient resolution (as good as 300 km s^{-1}) to partially resolve the coronal X-ray lines of FK Com, if they are as broad as the FUV hot lines, and a measurement of a 60–90 km s^{-1} Doppler shift of strong X-ray features (e.g., Table 3) is within the capabilities of HETGS (Ayres et al. 2001). In fact, Buzasi et al. (2003) have suggested that the bright Lyα emissions of hydrogenic neon and oxygen (at 12 and 18 Å, respectively) display excess broadening, but unfortunately, like the *FUSE* observation, the HETGS pointing was too short to achieve good S/N and adequate phase coverage. Highly broadened X-ray line shapes with time variable centroids would demonstrate that 10^7 K coronal gas threads extended structures with a patchy distribution in longitude, whereas narrow X-ray profiles would imply a more compact, near-surface arrangement.

Confirming one of these possibilities could play an important role in understanding the apparent abrupt transition in coronal morphology that accompanies evolution through the rapid braking phase, specifically the early stages of that process where FK Com surely finds itself today.

This work was supported by *FUSE* Guest Investigator grant NNG04GH25G and by NASA grant NAG5-13058. *FUSE* is operated by the Johns Hopkins University under NASA contract NAS5-32985. H. K. acknowledges Deutsche Forschungsgemeinschaft grant KO 2320/1. S. R. acknowledges Hubble Fellowship grant HST-HF-01190.01 from the Space Telescope Science Institute, operated by the Association of Universities for Research in Astronomy, Inc., under contract NAS 5-26555. This research also made use of the SIMBAD database, maintained by CDS, Strasbourg, France; the Multimission Archive at Space Telescope; and the Atomic Line List v2.04, hosted by the Department of Physics and Astronomy, University of Kentucky. The Nordic Optical Telescope is operated on the island of La Palma jointly by Denmark, Finland, Iceland, Norway, and Sweden, in the Spanish Observatorio del Roque de los Muchachos of the Instituto de Astrofisica de las Canarias.

REFERENCES

Ayres, T. R. 2006, in ASP Conf. Ser. 348, Astrophysics in the Far Ultraviolet: Five Years of Discovery with *FUSE*, ed. G. Sonneborn, W. Moos, & B.-G. Andersson (San Francisco: ASP), in press
Ayres, T. R., Brown, A., Osten, R. A., Huenemoerder, D. P., Drake, J. J., Brickhouse, N. S., & Linsky, J. L. 2001, ApJ, 549, 554
Ayres, T. R., Osten, R. A., & Brown, A. 1999, ApJ, 526, 445
Ayres, T. R., Simon, T., Stern, R. A., Drake, S. A., Wood, B. E., & Brown, A. 1998, ApJ, 496, 428 (A98)
Bianchi, L., Grewing, M., & Kappelmann, N. 1985, A&A, 149, 41
Bopp, B. W., & Rucinski, S. M. 1981, in IAU Symp. 93, Fundamental Problems in the Theory of Stellar Evolution, ed. D. Sugimoto, D. Q. Lamb, & D. N. Schramm (Dordrecht: Reidel), 177
Bopp, B. W., & Stencel, R. E. 1981, ApJ, 247, L131
Buzasi, D. L., Huenemoerder, D. P., & Preston, H. L. 2003, in The Future of Cool-Star Astrophysics: 12th Cambridge Workshop on Cool Stars, Stellar Systems, and the Sun, ed. A. Brown, G. M. Harper, & T. R. Ayres (Boulder: Univ. Colorado), 952
Deleuil, M., et al. 2005, A&A, 429, 247
de Medeiros, J. R., & Mayor, M. 1995, A&A, 302, 745
Dupree, A. K., Lobel, A., Young, P. R., Ake, T. B., Linsky, J. L., & Redfield, S. 2005, ApJ, 622, 629
Fabricius, C., & Makarov, V. V. 2000, A&A, 356, 141
Gondoin, P., Erd, C., & Lumb, D. 2002, A&A, 383, 919
Gray, D. F. 1981, ApJ, 251, 155
Green, J. C. 1998, Proc. SPIE, 3356, 265
Guinan, E. F., & Robinson, C. R. 1986, AJ, 91, 935
Harper, G. M., Wilkinson, E., Brown, A., Jordan, C., & Linsky, J. L. 2001, ApJ, 551, 486
Howk, J. C., Sembach, K. R., & Savage, B. D. 2003, ApJ, 586, 249
Huenemoerder, D. P., Ramsey, L. W., Buzasi, D. L., & Nations, H. L. 1993, ApJ, 404, 316 (H93)
Ilyin, I. V. 2000, Ph.D. thesis, Univ. Oulu
Innes, D. E., Inhester, B., Axford, W. I., & Willhelm, K. 1997, Nature, 386, 811
Innes, D. E., & Wang, T. 2004, in *SOHO* 13—Waves, Oscillations and Small-Scale Transient Events in the Solar Atmosphere: Joint View from *SOHO* and *TRACE*, ed. H. Lacoste (ESA SP-547; Noordwijk: ESA), 479
Jardine, M., & van Ballegooijen, A. A. 2005, MNRAS, 361, 1173
Jetsu, L., Pelt, J., & Tuominen, I. 1993, A&A, 278, 449
Korhonen, H., Berdyugina, S. V., Hackman, T., Strassmeier, K. G., & Tuominen, I. 2000, A&A, 360, 1067
Korhonen, H., Berdyugina, S. V., & Tuominen, I. 2002, A&A, 390, 179
Lenz, D. D., & Ayres, T. R. 1992, PASP, 104, 1104
Makarov, V. V., & Fabricius, C. 1999, A&A, 349, L34
Merrill, P. W. 1948, PASP, 60, 382

Moos, H. W., et al. 2000, ApJ, 538, L1
Parker, E. N. 1970, ARA&A, 8, 1
Piskunov, N., Wood, B. E., Linsky, J. L., Dempsey, R. C., & Ayres, T. R. 1997, ApJ, 474, 315
Piskunov, N. E., Tuominen, I., & Vilhu, O. 1990, A&A, 230, 363
Ramsey, L. W., Barden, S. C., & Nations, H. L. 1981, ApJ, 251, L101
Roberge, A., et al. 2001, ApJ, 551, L97
Sahnow, D. J., et al. 2000, ApJ, 538, L7
Simon, T., & Drake, S. A. 1989, ApJ, 346, 303
Strassmeier, K. G., Fekel, F. C., Bopp, B. W., Dempsey, R. C., & Henry, G. W. 1990, ApJS, 72, 191
Tandberg-Hanssen, E. 1995, The Nature of Solar Prominences (Boston: Kluwer)
Vogt, S. S., & Penrod, G. D. 1983, PASP, 95, 565
Wakker, B. P., et al. 2003, ApJS, 146, 1
Walter, F. M., & Basri, G. S. 1982, ApJ, 260, 735
Webb, D. F., Forbes, T. G., Aurass, H., Chen, J., Martens, P., Rompolt, B., Rusin, V., & Martin, S. F. 1994, Sol. Phys., 153, 73
Webbink, R. F. 1976, ApJ, 209, 829
Welty, A. D., & Ramsey, L. W. 1994, AJ, 108, 299
Welty, A. D., Ramsey, L. W., Iyengar, M., Nations, H. L., & Buzasi, D. L. 1993, PASP, 105, 1427
Wood, B. E., Linsky, J. L., & Ayres, T. R. 1997, ApJ, 478, 745
Zirker, J. B., Engvold, O., & Martin, S. F. 1998, Nature, 396, 440